

# Robust Nonlinear Adaptive Flight Control for Consistent Handling Qualities

Rolf Rysdyk and Anthony J. Calise, *Senior Member, IEEE*

**Abstract**—A flight control design is presented that combines model inversion control with an online adaptive neural network (NN). The NN cancels the error due to approximate inversion. Both linear and nonlinear NNs are described. Lyapunov stability analysis leads to the online NN update laws that guarantee boundedness. The controller takes advantage of any available knowledge for system inversion, and compensates for the effects of the remaining approximations. The result is a consistency in response which is particularly relevant in human operation of some unconventional modern aircraft. A tiltrotor aircraft is capable of converting from stable and responsive fixed wing flight to sluggish and unstable hover in helicopter configuration. The control design is demonstrated to provide a tilt-rotor pilot with consistent handling qualities during conversion from fixed wing flight to hover.

**Index Terms**—Adaptive control, flight control, neural network (NN), nonlinear control.

## SUMMARY

THE use of modern technology in flight control systems allows for the design of consistent handling qualities even during radical aircraft configuration changes. The same technology can also provide a fault tolerant control system that is capable of providing consistent handling while the vehicle is damaged. Although a number of ad hoc designs have been successfully demonstrated, their implementation by more conventional means lacks robustness and is prohibitively labor intensive.

Nonlinear Adaptive Control provides consistent performance that is superior to more conventional controller designs. It combines model inversion control with adaptive neural network (NN) compensation that cancels the inversion error. Both linear and nonlinear NNs are applied. Lyapunov stability analysis resembling conventional adaptive control determines the update laws. The nonlinear NN provides a more powerful application based on its universal approximation property. If an approximate model of the system is available, the controller architecture can take advantage of that information and compensates for the effects of approximation. When used in a model-following set-up, this results in consistent responses.

Manuscript received April 30, 2003; revised April 26, 2005. Manuscript received in final form May 17, 2005. Recommended by Associate Editor P. K. Menon.

R. Rysdyk is with the Department of Aeronautics and Astronautics, University of Washington, Seattle, WA 98195 USA (e-mail: rysdyk@aa.washington.edu).

A. J. Calise is with the School of Aerospace Engineering, Georgia Institute of Technology, Atlanta, GA 30332 USA (e-mail: anthony.calise@aerospace.gatech.edu).

Digital Object Identifier 10.1109/TCST.2005.854345

This aspect is desirable to reduce the workload of a human operator of complex systems like tiltrotor aircraft.

The tiltrotor aircraft is capable of converting from stable and responsive fixed wing flight to sluggish and unstable hover in helicopter configuration. It is desirable to provide the pilot with consistent handling qualities during a conversion from fixed wing flight to hover, which would typically occur during the high-workload landing phase of flight. A linear model inversion architecture is adopted by frequency separation. The architecture provides for a model following setup with guaranteed performance. A rigorous proof shows how boundedness is guaranteed.

## I. INTRODUCTION

Next generation aircraft may differ radically from their predecessors, presenting control designers with interesting challenges and opportunities. Examples include: low-observable and super-maneuverable tailless fighter aircraft like the X-36 in Fig. 1 and [1], aircraft capable of flight in multiple configurations like the tilt-rotor described in Section II-B, and remotely piloted and autonomous vehicles unconstrained by human occupants.

The desire for enhanced agility and functionality demands performance over an increased range of conditions characterized by large variations in dynamic pressure and aerodynamic phenomena. Furthermore, the use of nonlinear actuation systems increases the complexity of the control design. Alternatively, variation in response may occur due to damage or component failure, requiring rapid reconfiguration of the control system to maintain stable flight and reasonable levels of handling qualities. Therefore, there is interest in real-time direct adaptive control methods with guaranteed performance.

The most widely studied approach to nonlinear control involves the use of transformation techniques and differential geometry. The approach transforms the state and/or control of the nonlinear system into a linear representation. Linear tools can then be applied in terms of a pseudocontrol signal, which is subsequently mapped into the original coordinates via inverse transformation. This broad class of techniques is most commonly known as feedback linearization (FBL) [2]. FBL theory has many applications in flight control research. Meyer and Cicolani included the concept of a nonlinear transformation in their formal structure for advanced flight control [3]. Menon *et al.* used a two-time-scale approach to simplify the linearizing transformations [4]. A fixed Jacobian can provide a dynamic inverse for nonlinear plants, leading to asymptotic tracking of desired trajectories, with bounded error [5]. Dynamic inversion techniques have been investigated at great length for application to super-maneuverable aircraft [6]–[8]. A drawback of dynamic

inversion is its vulnerability to modeling errors [9]. Therefore, several techniques have been proposed to provide robustness to sources of uncertainty, which include unmodeled dynamics, parametric uncertainty, and uncertain nonlinearities [9]–[11].

Many of the results in adaptive control are derived from Lyapunov stability theory [12]. Although adaptive control has a long history, it did not gain favor until 1980, when important results guaranteeing closed-loop stability were obtained [13]. Several efforts concentrate specifically on direct adaptive control of feedback-linearizable systems [14], [15].

The sensitivity of some adaptive schemes to disturbances and unmodeled dynamics prompted investigation of robust adaptive control for linear systems. Possible tools include the use of a dead-zone to maintain bounded errors in the presence of noise [16], parameter projection techniques to provide robustness to unmodeled dynamics [17], and methods for improving robustness of adaptive nonlinear controllers using backstepping [18]. While treatment of disturbances and uncertain nonlinear functions is now common, fewer efforts address robustness to unmodeled dynamics. Some exceptions include application to high-performance aircraft [19], and use of the backstepping paradigm [20]–[22].

Artificial NNs have the ability to approximate continuous nonlinear functions [23], [24]. One advantage of the NN over simple table lookup approaches is the reduced amount of memory and computation time required. In addition, the NN can provide interpolation between training points with no additional computational effort. NNs function as nonlinear adaptive control elements and offer advantages over conventional linear parameter adaptive controllers. Survey papers commenting on the role of NN technology in flight control design have been contributed by Werbos [25] and Steinberg [26], [27]. We focus on the use of a direct adaptive NN-based control architecture that compensates for unknown nonlinearities in a feedback linearizing control framework. Previous works include applications to helicopters and tiltrotors [28]–[31], fighter aircraft [32], [33], agile missiles, and guided munitions [34]–[36]. In a second part of this paper, we address the issue of robustness to unmodeled actuator dynamics, which is treated by modifying the adaptation law with dynamic nonlinear damping [21], [35], which to our knowledge is the first time this has been developed for fully nonlinear adaptive systems.

## II. CONTROLLER ARCHITECTURE

### A. Approximate Inversion

The objective of this paper includes demonstration of the NN capability of adapting to errors caused by using an approximate inverse model. Unmodeled dynamics originate from the linearization used for the nominal inverting controller. This includes linearization of dynamics that are nonlinear with respect to the control variables. Additionally, any cross-coupling between fast rotational states and slow translational states is neglected in the inversion. In this paper, we consider the case where the number of outputs equal the number of available control inputs. By approximating the system dynamics to be linear in states and control variables, the approximate feedback



Fig. 1. Boeing/McDonnell Douglas X-36 tailless fighter agility research aircraft.

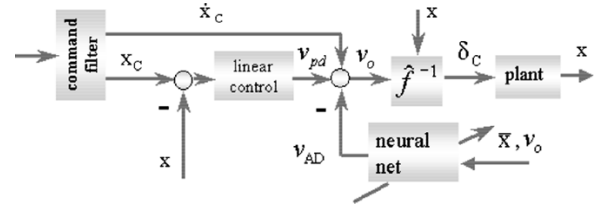


Fig. 2. Adaptive NN augmented model inversion architecture.

linearizing control design process reduces to construction of a model inverting control law. This control law represents a linear, state-dependent, transformation from pseudocontrol space to control space.

The conditions necessary for exact FBL of nonlinear systems are well researched [2]. Formal definitions for how “close” an approximate inverse model output is to the exactly linearized output are also known, including for model following control design [37]–[39]. A regulator can be added to the pseudocontrol to drive the error between actual output and model output to zero. Disturbances and variations in plant dynamics may be handled this way. Such methods have been successfully applied in flight control [40].

A rigorous justification for neglecting the moment-to-force coupling in aircraft dynamics in controller design is provided in an approximate input–output linearization theory in [41]. This paper is extended to tracking control for nonaffine systems in [42]. In our application, exact FBL will lead to linear behavior from pseudocontrol to vehicle-state. The use of an approximate model in the control law induces an *inversion error*. We consider here a definition of the inversion error as in [32].

Fig. 2 contains a diagram of the controller architecture. Consider the aircraft dynamics represented as

$$\dot{\mathbf{x}} = f(\mathbf{x}, \dot{\mathbf{x}}, \mathbf{u}). \quad (1)$$

Let  $\mathbf{u}^*$  represent an exact FBL control law. That is, the transformation  $\{\mathbf{x}, \boldsymbol{\nu}\} \rightarrow \{\mathbf{x}, \mathbf{u}^*\}$ , given by

$$\mathbf{u}^* = f^{-1}(\mathbf{x}, \dot{\mathbf{x}}, \boldsymbol{\nu}). \quad (2)$$

The transformation from pseudocontrol to state then becomes

$$\dot{\mathbf{x}} = \boldsymbol{\nu}. \quad (3)$$

Instead of control law (2), we apply an approximate transformation

$$\mathbf{u} = \hat{f}^{-1}(\hat{\mathbf{x}}, \dot{\hat{\mathbf{x}}}, \boldsymbol{\nu}) \quad (4)$$

where notation  $\hat{\mathbf{x}}(t)$  is used to distinguish these plant trajectories resulting from using  $\mathbf{u}(t)$  from those resulting from applying  $\mathbf{u}^*(t)$ . If  $f$  and  $\hat{f}$  are close, e.g., in the sense of [37] and [38], then  $\mathbf{x}(t)$  and  $\hat{\mathbf{x}}(t)$  will be close, and a regulator can be added to  $v$  to bring  $\hat{\mathbf{x}}(t) \rightarrow \mathbf{x}_c(t)$ . Using the approximate inversion control law (4), in light of these results, allows us to express the aircraft dynamics as follows:

$$\ddot{\hat{\mathbf{x}}} = f(\hat{\mathbf{x}}, \dot{\hat{\mathbf{x}}}, \mathbf{u}) = \hat{f}(\hat{\mathbf{x}}, \dot{\hat{\mathbf{x}}}, \mathbf{u}) + \Delta'_{\text{inv}} = \boldsymbol{\nu} + \Delta'_{\text{inv}} \quad (5)$$

where  $\Delta'_{\text{inv}}$  is the *inversion error* defined as

$$\Delta'_{\text{inv}} \triangleq f(\hat{\mathbf{x}}, \dot{\hat{\mathbf{x}}}, \mathbf{u}) - \hat{f}(\hat{\mathbf{x}}, \dot{\hat{\mathbf{x}}}, \mathbf{u}) \quad (6)$$

and  $\boldsymbol{\nu} = \boldsymbol{\nu}_o - \boldsymbol{\nu}_{\text{ad}}$ , with  $\boldsymbol{\nu}_{\text{ad}}$  representing the action of an adaptive NN designed to cancel  $\Delta'_{\text{inv}}$ . The closeness of the approximation is captured by the inversion error, which we may express in terms of the pseudocontrol signal as

$$\Delta'_{\text{inv}} = \Delta_{\text{inv}}(\hat{\mathbf{x}}, \dot{\hat{\mathbf{x}}}, \boldsymbol{\nu}) = f(\hat{\mathbf{x}}, \dot{\hat{\mathbf{x}}}, \hat{f}^{-1}(\hat{\mathbf{x}}, \dot{\hat{\mathbf{x}}}, \boldsymbol{\nu})) - \boldsymbol{\nu}. \quad (7)$$

The inversion error  $\Delta_{\text{inv}}$  depends on  $\boldsymbol{\nu}_{\text{ad}}$ , whereas  $\boldsymbol{\nu}_{\text{ad}}$  will be designed to cancel  $\Delta_{\text{inv}}$ . This poses a fixed-point problem with existence and uniqueness of its solution  $\boldsymbol{\nu}_{\text{ad}}$  guaranteed with the following assumption:

*Assumption 1:* The mapping  $\boldsymbol{\nu}_{\text{ad}} \mapsto \Delta_{\text{inv}}$  is a contraction over the entire input domain. This implies

$$\left| \frac{\partial \Delta_{\text{inv}}}{\partial \boldsymbol{\nu}_{\text{ad}}} \right| = \left| \frac{\partial (f - \hat{f})}{\partial \mathbf{u}} \frac{\partial \mathbf{u}}{\partial \boldsymbol{\nu}} \frac{\partial \boldsymbol{\nu}}{\partial \boldsymbol{\nu}_{\text{ad}}} \right| = \left| \frac{\partial (f - \hat{f})}{\partial \mathbf{u}} \frac{\partial \mathbf{u}}{\partial \hat{f}} \right| < 1$$

which can be stated as

$$\left| \left( \frac{\partial f / \partial \mathbf{u}}{\partial \hat{f} / \partial \mathbf{u}} \right) - 1 \right| < 1. \quad (8)$$

Expression (8) implies the following two conditions:

- 1)  $\text{sgn}(\partial f / \partial \mathbf{u}) = \text{sgn}(\partial \hat{f} / \partial \mathbf{u})$ ;
- 2)  $|\partial \hat{f} / \partial \mathbf{u}| > |\partial f / \partial \mathbf{u}| / 2 > 0$ .

### B. Tiltrotor Application

Tiltrotor aircraft combine the hover performance and control of a helicopter with the cruise speed and efficiency of a turboprop airplane. Tiltrotor aircraft feature wing-tip mounted prop-rotors that can be rotated from a vertical orientation for takeoff and landing to a horizontal position for efficient fixed-wing-borne flight for high-speed cruise, Fig. 3. There is an interest in large tiltrotor transports, which promise to relieve airport congestion by replacing commuter aircraft and freeing up runway slots.

The flight mechanics of a tiltrotor present both opportunities and challenges to the control designer. Prop-rotor movement from the vertical position in helicopter mode, toward the horizontal airplane mode position, rapidly accelerates the aircraft while orienting prop-rotor thrust to its optimum position. Conversely, up, and aft movement of the prop-rotors, required to prepare for a vertical landing, provides the drag needed to decelerate but at the same time produces undesirable additional lift, which the pilot must counteract with appropriate flight-path control.

Two common types of stability and control augmentation systems (SCAS) for aircraft are referred to as rate command attitude hold (RCAH) and attitude command attitude hold (ACAH)



Fig. 3. XV-15 tilt-rotor in helicopter configuration.

[43]. As outside visual cues degrade and flight-path precision requirements increase, as for example with civilian instrument meteorological conditions (IMC), the need arises for attitude stabilization and even attitude control for precise hovering and low-speed flight. As speed increases, the need for more roll maneuverability emerges, leading to a relaxation of roll control to a rate response type. Similarly, the desired control in yaw axis changes from heading command to yaw rate control with turn coordination (TC). The considerations involved in a tiltrotor IMC approach procedure, include [44]: a conversion schedule of nacelle angle with speed, from cruise to helicopter configuration in the approach, and *vice versa* for the missed approach procedure; deployment or retraction of flaps depending on nacelle angle, speed, and glide-slope; switching between control augmentation types, and; desired altitude and speed trajectories.

Consider the aircraft rotational dynamics represented by [45] and [46]

$$\dot{\boldsymbol{\omega}} = f(\mathbf{x}, \dot{\mathbf{x}}, \boldsymbol{\delta}_f) \quad (9)$$

where  $\mathbf{x} = [\mathbf{u} \ \mathbf{v} \ \mathbf{w} \ \phi \ \theta \ \psi]^T$  which are, respectively, the Cartesian components of velocity along the body-fixed axes and the Euler angles,  $\boldsymbol{\omega} = [p \ q \ r]^T$  contains the angular rates about the body-fixed axes, and  $\boldsymbol{\delta}_f = [\delta_{\text{lat}} \ \delta_{\text{lon}} \ \delta_{\text{dir}} \ \delta_{\text{col}}]^T$  is the control input, respectively, referred to as the lateral cyclic, longitudinal cyclic, rudder, and collective. The approximate model is based on dynamics linearized about a nominal operating point, with the rotor dynamics residualized

$$\dot{\boldsymbol{\omega}} = A_1 \mathbf{x}_1 + A_2 \boldsymbol{\omega} + B \boldsymbol{\delta} \quad (10)$$

where  $A_1, A_2$ , and  $B$ , respectively, represent the aerodynamic stability and control derivatives in the usual Jacobian sense. The collective/throttle control position is treated as one of the relatively slow translational states,  $\mathbf{x}_1 = [u \ v \ w \ \delta_{\text{col}}]^T$ . The inputs of interest are the controls of moments about the body axes,  $\boldsymbol{\delta} = [\delta_{\text{lat}} \ \delta_{\text{lon}} \ \delta_{\text{dir}}]^T$ .

The inverting control law is constructed from (10) by replacing the angular accelerations with their desired values  $\dot{\boldsymbol{\omega}}_D = [\dot{p}_D \ \dot{q}_D \ \dot{r}_D]^T$  and solving for the control perturbations. This results in the following control law:

$$\boldsymbol{\delta} = \hat{B}^{-1} \{ \dot{\boldsymbol{\omega}}_D - \hat{A}_1 \mathbf{x}_1 - \hat{A}_2 \boldsymbol{\omega} \} \quad (11)$$

where the hats indicate that we may allow some further uncertainty in approximations of  $A_1, A_2$ , and  $B$ . The inversion error is

$$\Delta_{\text{inv}} \triangleq \dot{\boldsymbol{\omega}} - (\hat{A}_1 \mathbf{x}_1 + \hat{A}_2 \boldsymbol{\omega} + \hat{B} \boldsymbol{\delta}). \quad (12)$$

The effect of  $\Delta_{\text{inv}}$  can be represented about the body-fixed axes as

$$\dot{\omega} = \dot{\omega}_D + \Delta_{\text{inv}}. \quad (13)$$

The components of  $\dot{\omega}_D$  are related to those of the pseudocontrol as explained next. The pseudocontrol for the three rotational degrees of freedom is designed in terms of body angular rates as

$$\nu = [\nu_p \ \nu_\theta \ \nu_{rr}]^T = \nu_o - \nu_{\text{ad}} \quad (14)$$

where  $\nu_{\text{ad}}$  is the output of a NN, and  $\nu_o$  is the output of a linear controller operating on a tracking error signal. A variety of linear control designs can be used to produce  $\nu_o$ . We use a combination of command filter and classic proportional–integral derivative (PID) control to provide the model following setup indicated in Fig. 2. If the poles of the command filter are co-located with those of the PID control, then in case of ideal inversion the architecture reduces to conventional explicit model following. With the approximate inversion, the PID control design affects the NN performance and, thus, determines the tracking error transient. The pseudocontrol signal  $\nu_o$  is designed as follows:

$$\nu_o = \begin{bmatrix} K_{P1}\tilde{p} + K_{I1}\tilde{\dot{p}} \\ K_{P2}\tilde{\theta} + K_{D2}\tilde{\dot{\theta}} \\ K_{P3}\tilde{r} + K_{I3}\tilde{\dot{r}} \end{bmatrix} + \begin{bmatrix} \dot{p}_c \\ \dot{\theta}_c \\ \dot{r}_c \end{bmatrix} \quad (15)$$

with

$$\dot{\tilde{p}} = \tilde{\dot{p}}, \quad \dot{\tilde{\rho}} = \tilde{\dot{r}} \quad (16)$$

where the signals  $\{p_c, \theta_c, r_c\}$  and their derivatives are the outputs from command filters, and for each component the tilde represents a command tracking error

$$\tilde{x} = x_c - x. \quad (17)$$

The command filters are used to specify the rotorcraft handling qualities [43]. In this paper, the signals  $\dot{p}_c$  and  $\dot{r}_c$  will be designed to provide RCAH in roll and yaw, and  $\dot{\theta}_c$  will provide ACAH in pitch. The integral action is added in the roll and yaw channels to provide the attitude hold in those channels. Integration and adaptation wind-up can be prevented with pseudocontrol hedging (PCH) [47]. Handling qualities specifications and actuator performance allow the tracking error transient to be fast relative to the dynamics of the command filter, while maintaining bandwidth separation from actuator dynamics. The following assumption can therefore be satisfied by design.

*Assumption 2:* Let the external commanded input and its first and second derivatives be bounded, for example such that

$$\|[\theta_c \ \dot{\theta}_c \ \ddot{\theta}_c]^T\| \leq \bar{\Theta}. \quad (18)$$

Similar assumptions are made for the roll and yaw channels. In what follows, a full three-axes control augmentation will be presented and demonstrated, while the pitch channel will be used as a detailed example for design and analysis. For the tiltrotor application, our focus is on the approach to landing phase of flight. The high workload associated with conversion from fixed-wing to helicopter flight combined with approach procedures calls for attitude-hold in all channels. The need for precision during the

approach-to-landing stages of flight benefits from attitude-command in the longitudinal channel. The roll and yaw channels are commonly designed for rate-command. The components of the desired acceleration  $\dot{\omega}_D$  for this combination of augmentation are related to the components of the pseudocontrol  $\nu$  as follows:

$$\dot{p}_D \equiv \nu_p \quad (19)$$

$$\dot{r}_D \equiv \nu_{rr}. \quad (20)$$

By using the derivative with respect to time of the pitch kinematic expressions, the desired angular acceleration about the body  $y$  axis can be solved for

$$\dot{q} = \frac{\ddot{\theta}}{c_\phi} + \dot{r}t_\phi + q\dot{\phi}\{t_\phi + r\} \quad \text{where} \quad (21)$$

$$\dot{\phi} = p + t_\theta\{qs_\phi + rc_\phi\} \quad (22)$$

where  $s_\phi$  is shorthand for  $\sin(\phi)$ , etc. Thus, the desired pitch rate, given the commanded attitude and yaw rate signals, is now seen to be

$$\dot{q}_D \equiv \frac{\nu_\theta}{c_\phi} + \nu_{rr}t_\phi + q\dot{\phi}\{t_\phi + r\}. \quad (23)$$

To see the effect of this construction on the inversion error, notice that by combination of (11), (12), and (23),  $\Delta_{\text{inv}}$  can be represented as a function of the states and the pseudocontrol. In pitch channel, the error is a function of  $\nu_\theta$  and  $\nu_{rr}$ . We may represent the effect of  $\Delta_{\text{inv}}$  in the Euler pitch-attitude dynamics as

$$\ddot{\theta} = \nu_\theta + \Delta_{\text{inv}}(2)c_\phi - \Delta_{\text{inv}}(3)s_\phi \quad (24)$$

where  $\Delta_{\text{inv}}(i)$  represents the  $i$ th component of vector  $\Delta_{\text{inv}}$ . Combining (14), (15), and (24), we obtain

$$\ddot{\theta} + K_D\dot{\theta} + K_P\theta = \nu_{\text{ad}}(2) - \Delta_\theta \quad (25)$$

where  $\Delta_\theta = \{\Delta_{\text{inv}}(2)c_\phi - \Delta_{\text{inv}}(3)s_\phi\}$  is the pitch component of the inversion error when represented in the Euler frame. The left-hand side of (25) represents the tracking-error dynamics. The right-hand side is the network compensation error, which acts as a forcing function on the tracking error dynamics. With perfect NN performance, the NN output  $\nu_{\text{ad}}(2)$  completely cancels  $\Delta_\theta$ .

### III. NEURAL NETWORK STRUCTURE

#### A. Linear NN Structure

An online NN is defined by its structure and its update laws. A linear NN structure consists of any linearly parameterized feedforward network that is capable of approximately reconstructing the inversion error. Reference [48] uses radial basis functions (RBFs) because these functions are universal approximators even when the network is linearly parameterized. However, it is well known that RBFs are poor at interpolation between their design centers, and a large number of such basis functions are needed for networks with multidimensional input vectors. In [32], RBFs were used to capture variations in Mach number, because in the trans-sonic region, these variations are difficult to represent by polynomial functions. In the current implementation, a single-layer sigma-pi network is used. The inputs to the network consist of the state variables, the pseudocontrol and a bias term. Fig. 4 shows a general depiction of a

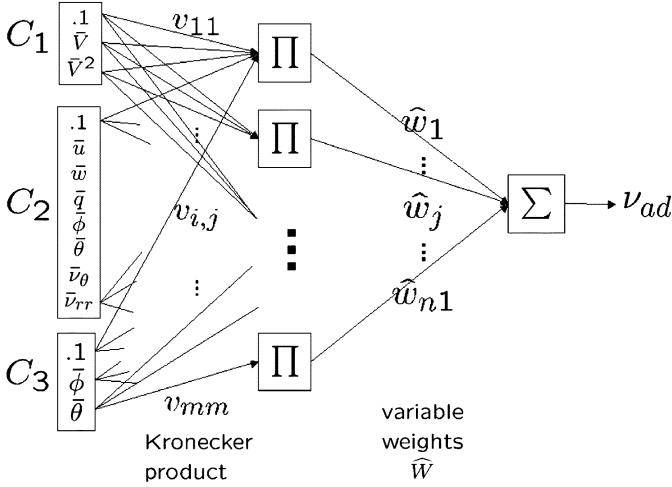


Fig. 4. Linear in the parameters *Sigma-Pi* NN structure designed for ACAH in the pitch channel.

sigma-pi network. The values  $v_{i,j}$  represent the weights associated with a nested kronecker product of input signal categories, and therefore they are (binary) constants. The values  $\hat{w}_j$  are the variable network weights.

The input–output map of the linear NN is represented as

$$\nu_{AD} = W^T \beta(\bar{x}, \bar{\nu}). \quad (26)$$

Here  $\nu_{AD}$  is the NN output,  $x$  and  $\nu$  are NN input, and the bar indicates possible normalization. The vector  $\bar{x}$  consists of selected normalized elements of the plant state and a bias term. The vector of basis functions  $\beta$  is akin to the regressor-vector in adaptive control texts. The basis functions are made up from a sufficiently rich set of functions so that the inversion error can be accurately reconstructed at the network output. The basis functions were constructed by grouping the normalized inputs into three categories. The first category is used to model inversion error due to changes in airspeed  $V = \sqrt{u^2 + v^2 + w^2}$ , since the (dimensional) stability and control derivatives are strongly dependent on dynamic pressure [45]. In allowing the plant to be nonlinear and uncertain in the control as well as in the states, the inversion error is a function of both state and control signals, and these are therefore contained in the second category. Furthermore, for error compensation in the pitch channel, both  $\nu_\theta$  and  $\nu_{rr}$  should be input. The third category is used to approximate higher order effects due to changes in pitch attitude. These are mainly due to the transformation between the body frame and the inertial frame

$$\begin{aligned} C_1 &: \{0.1, \bar{V}, \bar{V}^2\} \\ C_2 &: \{0.1, \bar{u}, \bar{w}, \bar{q}, \bar{\phi}, \bar{\nu}_\theta, \bar{\nu}_{rr}\} \\ C_3 &: \{0.1, \bar{\phi}, \bar{\theta}\}. \end{aligned}$$

Finally, the vector of basis functions is composed of combinations of the elements of  $C_1, C_2$ , and  $C_3$  by means of the Kronecker product

$$\beta = \text{kron}(\text{kron}(C_1, C_2), C_3)$$

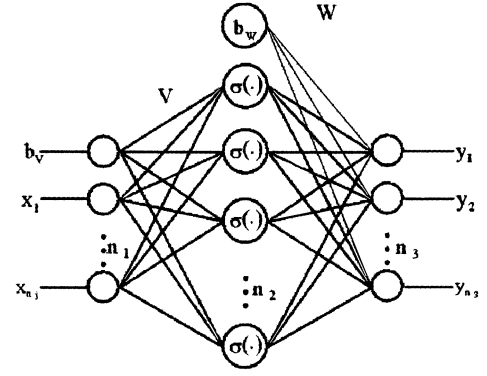


Fig. 5. Structure of a SHL perceptron network.

where

$$\text{kron}(x, y) = [x_1 y_1 \quad x_1 y_2 \quad \cdots \quad x_m y_n]^T.$$

The Kronecker product results in a combination of polynomial signals that will include  $\theta^2, \phi^2$ , and cross terms. The bias value in each class is normalized at 0.1, allowing for a pure bias component in  $\nu_{AD}$  of  $10^{-3}$  multiplied by  $\hat{w}_1$ .

### B. Nonlinear NN Structure

Consider again the architecture in Fig. 2. We now replace the linear-in-the-parameters NN with a single-hidden layer (SHL) “perceptron” NN. NNs with a SHL structure are more powerful than the linear NNs because they are universal approximators [23], [24]. Although the controller architecture does not reflect many changes from the linear NN application, there are differences in the stability analysis. Most of the added complexity can be traced back to the backpropagation update laws of the SHL-NN, and its associated Taylor-series approximation [49]. Fig. 5 shows the structure of a SHL perceptron NN. The input–output map of a SHL network can be represented as

$$y_k = b_w \theta_{wk} + \sum_{j=1}^{n_2} w_{jk} \beta_j \quad (27)$$

where  $k = 1, \dots, n_3$  and

$$\beta_j = \sigma \left( b_v \theta_{vj} + \sum_{i=1}^{n_1} v_{ij} x_i \right). \quad (28)$$

Here  $n_1, n_3$ , and  $n_2$  are, respectively, the number of input and outputs, and number of hidden layer neurons. The scalar function  $\sigma(z)$  is a sigmoidal activation function that represents the ‘firing’-characteristics of the neuron.

$$\sigma(z) = \frac{1}{1 + e^{-az}}. \quad (29)$$

The factor  $a$  is known as the *activation potential*. For convenience define the two weight matrices

$$V = \begin{bmatrix} \theta_{V1} & \cdots & \theta_{Vn2} \\ V_{1,1} & \cdots & V_{1,n2} \\ \vdots & \ddots & \vdots \\ V_{n1,1} & \cdots & V_{n1,n2} \end{bmatrix}$$

and

$$W = \begin{bmatrix} \theta_{W1} & \cdots & \theta_{Wn3} \\ W_{1,1} & \cdots & W_{1,n3} \\ \vdots & \ddots & \vdots \\ W_{n2,1} & \cdots & W_{n2,n3} \end{bmatrix}.$$

It is also convenient to define a vector  $\beta(\mathbf{z})$  as

$$\beta(\mathbf{z}) \doteq [b_W \ \sigma(z_1) \ \sigma(z_2) \ \cdots \ \sigma(z_{n2})]^T \quad (30)$$

where  $b_W \geq 0$  allows for the thresholds  $\theta_W$  to be included in the weight matrix  $W$ . Define

$$\bar{\mathbf{x}} \doteq [b_V \ \mathbf{x}]^T \quad (31)$$

$b_V \geq 0$  is an input bias that allows for the thresholds  $\theta_V$  to be included in the weight matrix  $V$ . With the previous definitions, the input–output map of a SHL Perceptron can be written in matrix form as

$$y = W^T \beta(V^T \bar{\mathbf{x}}). \quad (32)$$

The representation of the NN output given in (32), may be used to represent a linear-in-the-parameters NN by specifying  $V \equiv I$ , and constructing  $\beta(\mathbf{z})$  by using well distributed radial basis-functions [48], or by providing polynomial combinations of the elements of  $\mathbf{z}$  [28].

#### IV. INVERSION ERROR COMPENSATION

Consider a NN approximation of an inversion error

$$W^{*T} \beta(V^{*T} \bar{\mathbf{x}}) = \Delta_{\text{inv}}(\bar{\mathbf{x}}) - \varepsilon(\bar{\mathbf{x}}) \quad (33)$$

where  $0 \leq \|\varepsilon\| \leq \bar{\varepsilon}$ , where  $\bar{\varepsilon}$  an upperbound defined in what follows. The vector  $\varepsilon$  is referred to as the NN *reconstruction error*, or *residual error*. The vector  $\beta$  provides the set of basis functions that serves to approximate the function  $\Delta_{\text{inv}}$ . We may include adaptive parameters in this set, as is the case with perceptron NNs, resulting in nonlinearly parameterized NN output. The NN input  $\bar{\mathbf{x}}$  is made up of selected elements of the state vector and pseudocontrol. The selection of the elements of  $\bar{\mathbf{x}}$  is done through careful assessment of the inversion error [28].  $W^*$ , and  $V^*$  are matrices of constant, not necessarily unique, parameter values that minimize  $\|\varepsilon\|$ . These parameters are ideal, for example in the sense that, in a domain  $\mathcal{D}_e$  of  $\bar{\mathbf{x}}$ , they bring the term  $W^{*T} \beta(V^{*T} \bar{\mathbf{x}})$  to within a  $\varepsilon$ -neighborhood of the error  $\Delta_{\text{inv}}$ , where  $\varepsilon$  is bounded by

$$\bar{\varepsilon} \equiv \sup_{\bar{\mathbf{x}} \in \mathcal{D}_e} |W^{*T} \beta(V^{*T} \bar{\mathbf{x}}) - \Delta_{\text{inv}}(\bar{\mathbf{x}})|. \quad (34)$$

Thus,  $W^*$  and  $V^*$  may be defined to be values of  $W$  and  $V$  that minimize  $\bar{\varepsilon}$  over  $\mathcal{D}_e$ . The online NN output may be represented as

$$\nu_{\text{ad}} = W^T \beta(V^T \bar{\mathbf{x}}) \quad (35)$$

where  $W$  and  $V$  are the estimates of the ideal parameters. We need to make the following assumption. Define

$$Z = \begin{bmatrix} V & 0 \\ 0 & W \end{bmatrix} \quad (36)$$

and let  $\|\cdot\|$  imply the Frobenius norm.

*Assumption 3:* The norm of the ideal NN weights is bounded by a known positive value

$$\|Z^*\| \leq \bar{Z}. \quad (37)$$

Let  $\tilde{W}$  and  $\tilde{V}$  be the estimates of, respectively,  $W^*$  and  $V^*$ . Define  $\tilde{W} = W - W^*$ ,  $\tilde{V} = V - V^*$  and define the hidden-layer output approximation error as

$$\tilde{\beta} = \beta - \beta^* \doteq \beta(V^T \bar{\mathbf{x}}) - \beta(V^{*T} \bar{\mathbf{x}}). \quad (38)$$

To backpropagate the estimation error through the NN hidden-layer, we use a Taylor series expansion about the current estimate of the hidden layer output,  $\beta(\hat{\mathbf{z}}) = \beta(V^T \bar{\mathbf{x}})$ , where we are specifically interested in  $\mathbf{z} = \mathbf{z}^* = V^{*T} \bar{\mathbf{x}}$

$$\beta^* = \beta - \beta_z(V^T \bar{\mathbf{x}}) \tilde{V}^T \bar{\mathbf{x}} + \mathcal{O}(\tilde{V}^T \bar{\mathbf{x}})^2 \quad (39)$$

where

$$\beta_z(\hat{\mathbf{z}}) \triangleq \left. \frac{d\beta(\mathbf{z})}{d\mathbf{z}} \right|_{\mathbf{z}=\hat{\mathbf{z}}} = \begin{bmatrix} 0 & \cdots & 0 \\ \frac{\partial \sigma(z_1)}{\partial z_1} & \cdots & \frac{\partial \sigma(z_1)}{\partial z_{n2}} \\ \vdots & \vdots & \vdots \\ \frac{\partial \sigma(z_{n2})}{\partial z_1} & \cdots & \frac{\partial \sigma(z_{n2})}{\partial z_{n2}} \end{bmatrix}_{\mathbf{z}=\hat{\mathbf{z}}} \quad (40)$$

and  $\hat{\mathbf{z}} = [\hat{z}_1 \ \hat{z}_2 \ \cdots]^T$ .

*Remark 1:* As an example, consider the second-order error dynamics in the pitch channel (25), which may be represented as

$$\dot{\mathbf{e}} = \mathbf{A}\mathbf{e} + \mathbf{b}(\nu_{\text{ad}}(2) - \Delta_\theta) \quad (41)$$

where

$$\mathbf{A} = \begin{bmatrix} 0 & 1 \\ -K_P & -K_D \end{bmatrix}$$

and  $\mathbf{b} = [0 \ 1]^T$ , and with

$$\mathbf{e} = \begin{pmatrix} \tilde{\theta} \\ \dot{\tilde{\theta}} \end{pmatrix}. \quad (42)$$

*Remark 2:* Due to nonaffinity of the plant with respect to control, the inversion error,  $\Delta_{\text{inv}}$ , is in general a function of the pseudocontrol, which includes the output of the NN. Since the output of the NN is providing compensation for the inversion error, a fixed point problem occurs. To insure that Assumption 1 holds,  $\nu$  is input to the NN through a squashing function.

*A. Using the Nonlinear NN for Inversion Error Compensation*

If the nonlinear NN is used, the signal  $\nu_{\text{ad}}$  is designed as

$$\nu_{\text{ad}} = W^T \beta(V^T \bar{\mathbf{x}}) + \nu_r \quad (43)$$

where  $\mathbf{v}_r$  is a term that robustifies against the effects of higher order terms in the Taylor series approximation in (39)

$$\mathbf{v}_r = -K_r(\|Z\| + \bar{Z}_o)\zeta \quad (44)$$

where  $K_r > c_3, c_3$  a known positive constant defined later, and  $\bar{Z}_o$  such that  $\|Z^* - Z_o\| < \bar{Z}_o$ . The update law of the NN weights is designed as

$$\dot{W} = \dot{\hat{W}} = -\{(\boldsymbol{\beta} - \boldsymbol{\beta}_z V^T \bar{\mathbf{x}})\zeta + \lambda|\zeta|(W - W_o)\}\Gamma_w \quad (45)$$

$$\dot{V} = \dot{\hat{V}} = -\{\bar{\mathbf{x}}\zeta W^T \boldsymbol{\beta}_z + \lambda|\zeta|(V - V_o)\}\Gamma_v \quad (46)$$

where  $\Gamma_v, \Gamma_w > 0$ , and  $\lambda > c_2, c_2$  a known positive constant defined later. The damping term  $\lambda|\zeta|(Z - Z_o)$  is known as *e-modification*. In our design,  $\Gamma_w = \gamma_w I_w, \Gamma_v = \gamma_v I_v$  with  $\gamma_v, \gamma_w > 0$ . The elements of  $\boldsymbol{\beta}_z$  represent the sensitivity of the hidden layer to its input, for the nonlinear NN  $\boldsymbol{\beta}_z = \boldsymbol{\beta}_z(V^T \bar{\mathbf{x}})$ . The scalar  $\zeta$  is the filtered error term

$$\zeta = \mathbf{e}^T P \mathbf{b} \quad (47)$$

with for the second-order example in the pitch channel

$$P = \begin{bmatrix} \frac{K_D}{K_P} + \frac{1}{2K_D} & \frac{1}{2K_P} \\ \frac{1}{2K_P} & \frac{1+K_P}{2K_P K_D} \end{bmatrix} = \begin{bmatrix} P_{11} & P_{12} \\ P_{12} & P_{22} \end{bmatrix}.$$

### B. Using the Linear NN for Inversion Error Compensation

If a linear-in-the-parameters NN is used with  $V \equiv I$ , i.e., linear in the adaptive parameters  $W$ , then no update of  $V$  is desired,  $\boldsymbol{\beta}_z = 0$ , and  $\boldsymbol{\beta}^* \equiv \boldsymbol{\beta}$  therefore  $\mathbf{v}_r = 0$ , and

$$\mathbf{v}_{\text{ad}} = W^T \boldsymbol{\beta}(\bar{\mathbf{x}}). \quad (48)$$

The adaptation law is given, with  $\gamma > 0$ , by

$$\dot{W} = \dot{\hat{W}} = -\gamma\{\zeta \boldsymbol{\beta} + \lambda|\zeta|(W - W_o)\}. \quad (49)$$

*Remark 3:* The example provides for ACAH in the longitudinal channel, i.e., a design with second-order tracking error dynamics. This design may be generalized with

$$\mathbf{e} = [\hat{x}^{(n)} \quad \hat{x}^{(n-1)} \quad \dots \quad \hat{x}]^T \quad (50)$$

and  $\mathbf{b} = [0 \quad \dots \quad 0 \quad 1]^T$  a size- $n$  vector, and  $P$  an  $n \times n$ -matrix that solves  $A_n^T P + P A_n - 2I_n = 0$ , with  $A_n$  in canonical form similar to (42), expanded to order  $n$ .

*Remark 4:* Equations (45), (46), (44), and (49) are stated for a single channel setup, i.e., with one NN output. The statements may be generalized for MIMO implementation. In fact, the strength of the architecture lies in the cancellation of a nonlinear and possibly multidimensional inversion error which may include coupling of multiple states and control effects. A MIMO application that takes advantage of this capability is detailed in [50].

### C. Filtered Error Bound

Let  $\|\cdot\|$  imply the two-norm in case of vectors and the Frobenius norm in case of matrices. The construction of  $\zeta$  in (47) can be seen as an *error filter*, see the Appendix. From the

Cauchy–Schwarz inequality and the compatibility of the Frobenius norm with the vector 2-norm, it is clear that  $\zeta$  is bounded if  $\mathbf{e}$  is

$$|\zeta| \leq \|\mathbf{e}\| \|P\|. \quad (51)$$

A bounded  $\zeta$  also implies a bound on the 2-norm of  $\mathbf{e}$ , allowing concentration on the boundedness of the scalar  $\zeta$  [2].

*Lemma 1:* Let  $\zeta$  be constructed as (47), and suppose  $\zeta \leq \bar{\zeta}$  then

$$|\hat{\theta}(t)| \leq \frac{1}{P_{12}} \bar{\zeta}(t) \quad (52)$$

and

$$|\dot{\hat{\theta}}(t)| \leq \frac{2}{P_{22}} \bar{\zeta}(t). \quad (53)$$

A proof is given in the Appendix. From Lemma 1, we can obtain

$$\|\mathbf{e}\|^2 = |\hat{\theta}|^2 + |\dot{\hat{\theta}}|^2 \leq \left( \frac{1}{P_{12}^2} + \frac{4}{P_{22}^2} \right) \bar{\zeta}^2. \quad (54)$$

### D. Guaranteed Boundedness

The NN input design is discussed in the Appendix. The NN input can be upper bounded in terms of the tracking performance by

$$\|\bar{\mathbf{x}}\| \leq c'_o + c'_1 |\zeta| + c'_2 \|\tilde{Z}\|$$

where  $c'_i > 0$  are known. From (39)

$$\mathcal{O}(\tilde{V}^T \bar{\mathbf{x}})^2 = -\tilde{\boldsymbol{\beta}} + \boldsymbol{\beta}_z \tilde{V}^T \bar{\mathbf{x}}$$

where  $\boldsymbol{\beta}_z = \boldsymbol{\beta}_z(V^T \bar{\mathbf{x}})$ . With these results the higher order terms associated with the back propagation are bounded from above by

$$\|\mathcal{O}(\tilde{V}^T \bar{\mathbf{x}})^2\| < c'_3 + c'_4 \|\tilde{Z}\| \|\bar{\mathbf{x}}\| \quad (55)$$

where  $c'_i > 0$ , known. Let  $w$  be defined as the NN approximation error plus the higher order effects of back propagation through the nonlinear NN:

$$w = \varepsilon + W^* \mathcal{O}(\tilde{V}^T \bar{\mathbf{x}})^2 + \tilde{W}^T \boldsymbol{\beta}_z V^{*T} \bar{\mathbf{x}}.$$

Considering the properties of the NN structure, (55), and (34), an upper bound on  $w$  in terms of  $\|\tilde{Z}\|$  is

$$|w| < C'_0 + C'_1 \|\tilde{Z}\| \|\bar{\mathbf{x}}\|.$$

Combining this with (A-4), then

$$|w| < c_0 + c_1 \|\tilde{Z}\| + c_2 \|\tilde{Z}\|^2 + c_3 \|\tilde{Z}\| |\zeta| \quad (56)$$

where  $c_i > 0$  are known.

*Remark 5:* Using the facts that

$$\|\tilde{Z}\| \leq \bar{Z} + \|Z\| \quad \text{and} \quad \|\tilde{Z}\|^2 \leq \bar{Z}^2 + \|Z\|^2 + 2\bar{Z}\|Z\|$$

it is possible to find a known upper bound  $\bar{w}$  such that

$$|w| < \bar{w} = C_0 + C_1 \|Z\| + C_2 |\zeta| + C_3 \|Z\| |\zeta| + C_4 \|Z\|^2. \quad (57)$$

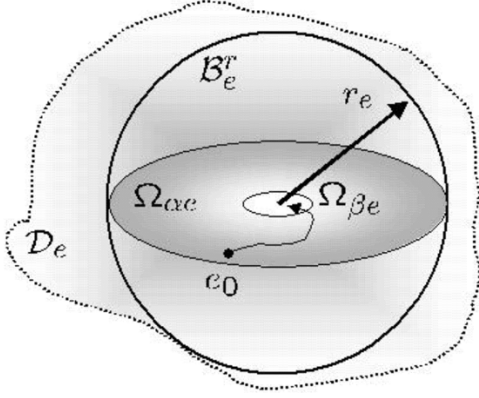


Fig. 6. Geometric representation of sets in the theorem.

In the formulation of this control problem, the error space can be considered as consisting of a subspace associated with tracking, and one associated with the NN weights. In the tracking error subspace, let

$$B_e^r = \{\mathbf{e} : \|\mathbf{e}\| \leq r_e\}. \quad (58)$$

Let  $\bar{\lambda}_P$  and  $\underline{\lambda}_P$  represent, respectively, the maximum and minimum eigenvalue of positive-definite matrix  $P$ . Let  $\Omega_{\alpha e}$  be defined by, Fig. 6

$$\Omega_{\alpha e} \triangleq \{\mathbf{e} \in B_e^r : \mathbf{e}^T \bar{P} \mathbf{e} \leq \alpha_e\} \quad (59)$$

where

$$\alpha_e = \min_{\|\mathbf{e}\|=r_e} \mathbf{e}^T \bar{P} \mathbf{e} = r_e^2 \underline{\lambda}_P. \quad (60)$$

Similarly, in the NN weight subspace with learning rate  $\Gamma = \gamma I$ , where  $I$  the identity matrix of appropriate dimension, let

$$B_z^r = \{\tilde{Z} : \|\tilde{Z}\| \leq r_z\} \quad (61)$$

and  $\Omega_z \triangleq \{\tilde{Z} \in B_z^r\}$ .

*Theorem 1:* If  $\{\mathbf{e}(t_0), \tilde{Z}(t_0)\} \in \{\Omega_{\alpha e}, \Omega_z\}$  and if the domain  $\mathcal{D}_e$  of  $\bar{\mathbf{x}}$  is sufficiently large, such that  $B_e^r \subset \mathcal{D}_e$ , with

$$r_e > \{c_0 + (\lambda - c_2)a^2\} \sqrt{\frac{\bar{\lambda}_P^3}{\underline{\lambda}_P}} \quad (62)$$

and similarly, the domain  $\mathcal{D}_z$  of  $\tilde{Z}$  sufficiently large such that  $B_z^r \subset \mathcal{D}_z$  with

$$r_z > a + \sqrt{a^2 + \frac{c_0}{\lambda - c_2}} \quad (63)$$

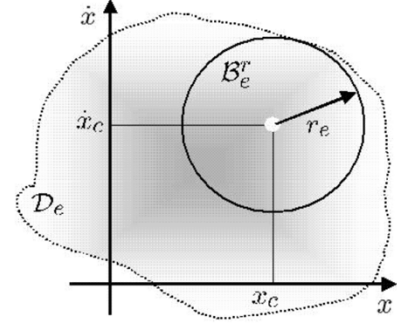
where  $a = (1/2)(c_1 + \lambda \bar{Z}_o)/(\lambda - c_2)$ , then all the signals in a system defined by (41) and (49) will remain bounded.

A proof is presented in the Appendix.

*Remark 6:* The term  $\bar{w}$  represents the effects of back propagation, which is not applicable to the linear NN. For the linear NN,  $Z \equiv W$ , therefore

$$r_e > \{\bar{\varepsilon} + \lambda \bar{W}_o^2/4\} \sqrt{\frac{\bar{\lambda}_P^3}{\underline{\lambda}_P}}. \quad (64)$$

*Remark 7:* The external command signals were assumed to be bounded, as in Assumption 2. The effect of these command


 Fig. 7. Geometric representation of the effect of  $r_e(\lambda \bar{Z}_o)$  on the allowable commands.

signals can be pictured in a geometric representation of the intersection of the sets with the  $\mathbf{e}$ -subspace, Fig. 7. This shows that commands of larger magnitude imply smaller values for  $\gamma$ . This may be interpreted to mean that to limit the closed-loop bandwidth, smaller NN learning rates may be required when allowing for more aggressive command tracking.

## V. TILT-ROTOR SIMULATION RESULTS

The aircraft is simulated using the real time flight simulation model of a tilt-rotor aircraft Generic Tilt-Rotor Simulator (GTRS) developed at the NASA Ames Research Center in support of the XV-15 and V-22 programs [51]. The code was extended to include actuator dynamics and nonlinearities. The following results summarize the controller performance in all channels. In the designs for human piloting investigated here, both the linear and SHL NN performed similarly, with only minor differences due to NN sizing and learning rate. It should be noted however that in more aggressive and highly nonlinear applications, the SHL NN has been demonstrated to have superior performance [1], [36], [52].

### A. Command Filter Design

The GTRS code includes the existing XV-15 control augmentation, here referred to as *original SCAS*. This SCAS is gain scheduled with speed and with mast-angle. In the longitudinal channel, it provides ACAH and RCAF, depending on the mode selected by the pilot. The ACAH setting was used for the comparison in the following results. The linear PID controller dynamics in (15) were designed so that the NN error settles within 0.5 s.

If the model following performance in the architecture of Fig. 2 is guaranteed over the frequencies of interest for handling qualities (0.2–6.0 rad/s), the Airworthiness Design Standard ADS-33D requirements [43] can be implemented by means of, respectively, a second- and first-order command filter. In that case, the Lyapunov stability offers a guarantee of the ADS-33 performance. Attitude Command can then be implemented with a second-order pitch-angle command filter, such that its dominant complex poles provide minimal overshoot and a 5% settling time of 1.5 s. This provides Level 1 handling characteris-

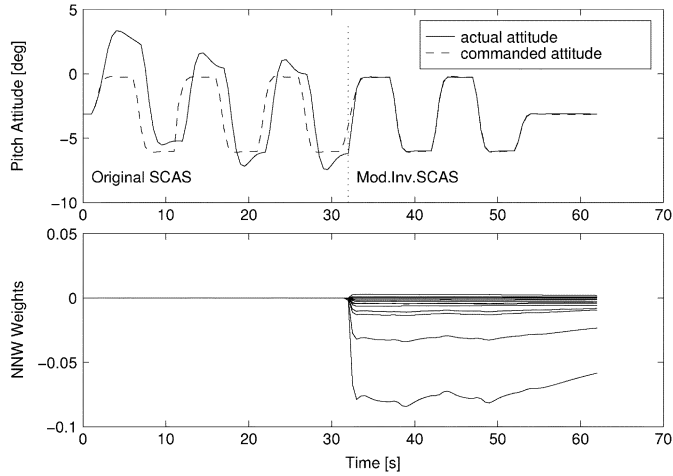


Fig. 8. Longitudinal SCAS comparison. The aircraft starts out trimmed at nominal-operating configuration. During the first 30 s it responds using the original gain scheduled SCAS. The aircraft remains within 10 Kts and within 250 ft of its altitude. At  $t = 32$  the model inversion SCAS is activated as evidenced by the NN weight histories.

tics in the pitch channel. Level 1 Rate Command handling qualities in roll has a phase bandwidth  $\omega_{BW} > 2$  rad/s. With the roll-yaw coupling small, the time constant of the roll response is approximately the inverse of the bandwidth, therefore

$$K_{cf} \geq \frac{1}{\tau_p} \approx \omega_{BW}. \quad (65)$$

This provides the roll command filter with a 5% settling time of approximately 1.5 s. The setup for the yaw-channel is similar with a time constant,  $\tau_r = 0.25$  s. These command filter designs will provide Level 1 handling qualities when the augmented aircraft can indeed follow the command filter dynamics up to these frequencies.

### B. Control Augmentation for the Longitudinal Channel

A comparison of the original SCAS with the NN augmented model inversion augmentation is presented in Fig. 8. The improvement in pitch response is clearly visible. The same performance was obtained at various points in the operation envelope and at various configurations, including at 35 000 ft in aircraft configuration. The augmentation in the lateral channel is able to provide similar performance and consistency in response. To further evaluate the performance of the NN adaptive control, a pilot model was developed [53]. The pilot model is able to follow desired altitude, speed, and conversion profiles, Fig. 9. Note that the NN weight histories return toward nominal as the tiltrotor is maneuvered back to trim.

### C. Control Augmentation for the Lateral Channels

Two common modes of augmentation in the yaw channel are heading hold (HH) and TC. In a tiltrotor aircraft, a transition between these modes is typically made between 25 and 45 Kts. HH is inherent to the controller architecture as attitude stabilization in yaw. TC pertains to the need for coupling between the roll and yaw motion to provide for a comfortable and efficient change in heading. Etkin [45] defines a *coordinated turn* as a turn wherein the rate of change in heading is constant, and the resultant of gravity and centrifugal force at the center of mass lies in the

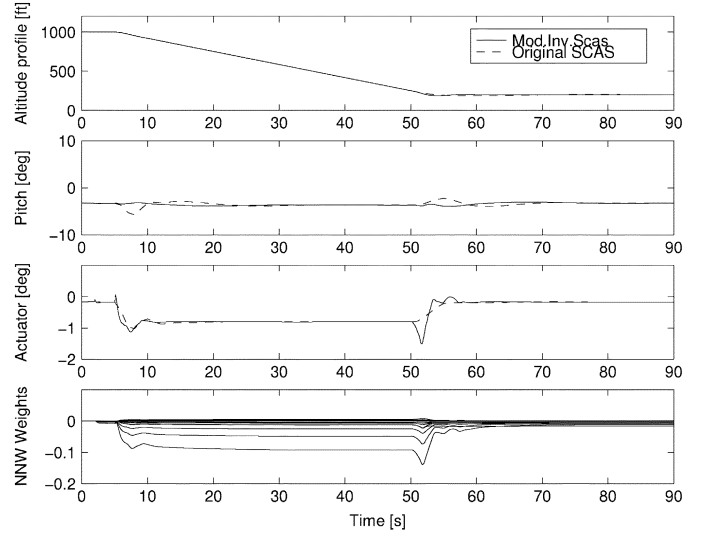


Fig. 9. Simulated approach to minimum descent altitude, starting from 1000 ft in nominal operating configuration at 30 Kts helicopter configuration. The desired descent rate is 1000 fpm. The primary control for establishing the descent rate is the collective. This has an effect on the velocity, which is subsequently controlled by the pilot model through pitch commands. Note that the NN weight histories return toward nominal as the tiltrotor is maneuvered back to trim.

plane of symmetry. This definition approximates closely a piloted flight on the *turn-and-bank* indicator. For the implementation of TC, only the command filter dynamics are considered, i.e., we assume perfect tracking of yaw rate command. The desired yaw rate can then be expressed as

$$r_{com} = \frac{1}{u} \{K_P(a_{Ycom} - a_Y) + wp + gs_\phi c_\theta\} \quad (66)$$

where  $K_P$  is the gain of the tracking dynamics in the roll-channel, and  $a_Y$  is the acceleration along the body- $y$  axis. The dynamics due to  $\dot{v}$  are neglected as its value is usually not available from measurement. For the guidance outerloop we take the yaw rate to respond as directed by a first-order command filter. Grouping the  $\dot{v}$  dynamics with the difference between measured and actual effects of roll-rate and gravity, as

$$\Delta_Y = \dot{v} - \left\{ \frac{\tau_r s}{\tau_r s + 1} \right\} (wp + gs_\phi c_\theta). \quad (67)$$

Equation (67) indicates that the effects of gravity and roll rate are washed out. The effects due to  $\dot{v}$  are not, but if  $a_{Ycom} = 0$  and with mild maneuvering, this augmentation will keep  $a_Y$  suppressed. Closing the loop results in an expression for the lateral-acceleration transients

$$a_Y = \frac{K_P}{\tau_r s + (1 + K_P)} a_{Ycom} + \frac{\tau_r s + 1}{\tau_r s + (1 + K_P)} \Delta. \quad (68)$$

Fig. 10 compares the performance of the original XV-15 SCAS with the model inversion controller. The original augmentation provides rate command and attitude command with attitude retention (ACAH) upon selection. No HH or automatic TC is available for comparison. Figs. 11, and 12 demonstrate the augmented response in the lateral channels given.

The controller architecture inherently provides for HH. Fig. 13 displays the difference in performance between TC and HH mode. HH would typically be used at speeds below 45 Kts,

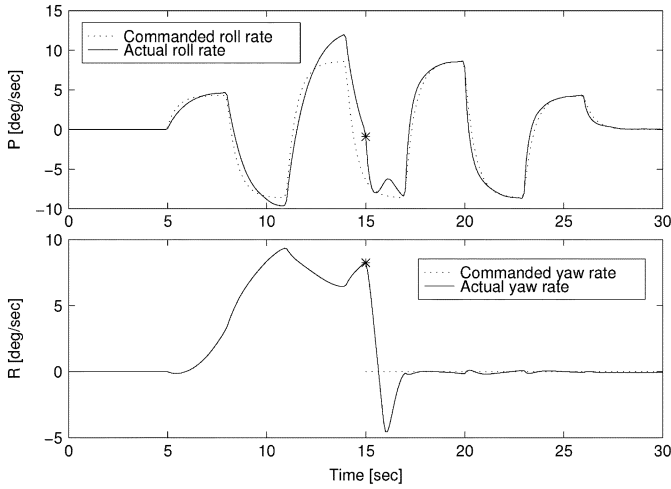


Fig. 10. Lateral SCAS comparison; response to a square wave lateral stick input at hover, at 5000 ft. The original SCAS is active until  $t = 15$  s, at that moment the model inversion SCAS is switched on. The 2-s fluctuation in roll rate is due to the coupling of the yaw augmentation that is now providing HH.

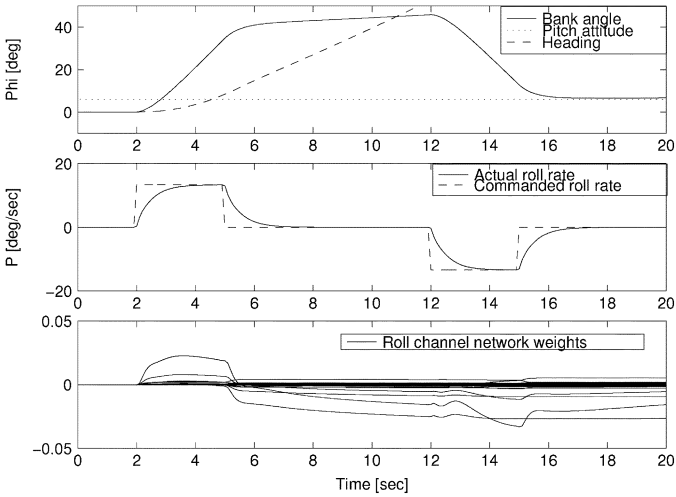


Fig. 11. Roll channel command and response to roll rate doublet, with automatic TC, leading to a  $45^\circ$  banked turn. The tiltrotor is flying 170 Kts, at 10000 ft, in cruise configuration. Automatic TC is implemented as in (66), with  $a_{Y\text{com}} = 0g$ .

TC is used in cruise flight. The 30 Kts flight is representative for HH operation, but rather an extreme for the TC mode. The controller is able to provide good performance.

D. Handling Qualities

ADS-33D [43] requirements have a specific focus, in each channel on: small amplitude (high frequency) responses; moderate and large amplitude responses; and response to disturbance (attitude hold performance) [31], [54]. The simulation model includes XV-15 actuator dynamics and nonlinearities. However, the investigated maneuvers did not lead to actuator saturation. The small amplitude response to control inputs is tested through a frequency sweep,  $0.2 \rightarrow 6.0$  rad/s. The unaugmented XV-15 displays conventional first-order roll rate characteristics where aileron deflections produce a proportional roll rate at low frequencies, and acceleration at high frequencies. The dominant time constant is approximately 1 s. The critical bandwidth is determined by the  $45^\circ$  phase margin [43]. The effective phase time

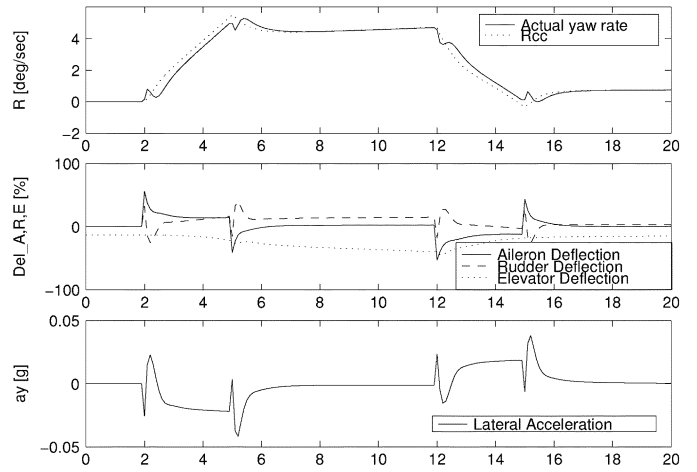


Fig. 12. Yaw channel response, control surface deflections and TC performance in roll rate doublet of Fig. 11.

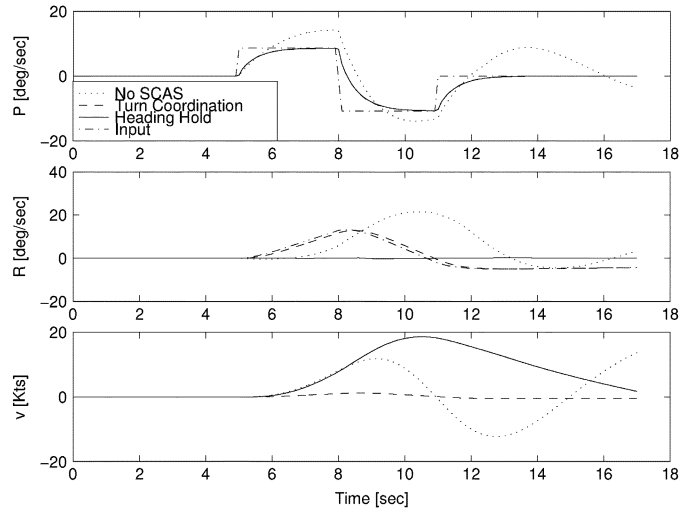


Fig. 13. HH versus TC in helicopter configuration, 30 Kts at 3000 ft. Given a doublet roll rate command, the performance in roll channel shows no differences. The maximum bank angle is approximately  $25^\circ$ . In HH mode, the heading remains within  $0.25^\circ$  of its trim value, and the aircraft reaches a lateral velocity of 20 Kts.

delay is negligible since the phase curve is nearly flat where it is near  $180^\circ$ . The bandwidth-phase-delay requirement, for Level 1 roll response, is similar to the one in pitch response, referred to as *Small Amplitude Roll Attitude Changes*. It is a requirement for a phase bandwidth of  $\omega_{BW\theta} > 2$  rad/s. If the roll-yaw coupling is small then the time constant of the roll response is approximately the inverse of the phase bandwidth,  $\tau_p \approx (1)/(\omega_{BW\theta})$ . So a command filter design with a time constant  $\tau_p < 0.5$  s should result in Level 1 handling qualities. Fig. 14 shows the results of the frequency sweep. Moderate amplitude changes (*attitude quickness*) requirements and Level 1 requirements for so-called *large amplitude roll attitude changes* for IMC operations were also achieved [54].

Figs. 15, and 16 give the pitch response to a longitudinal square wave stick input. The XV-15 is flying at 2000', at approximately 100 Kts, in helicopter configuration. The figures contrasts the commanded pitch angle with the response using model inversion only, using the linear NN, and using the SHL

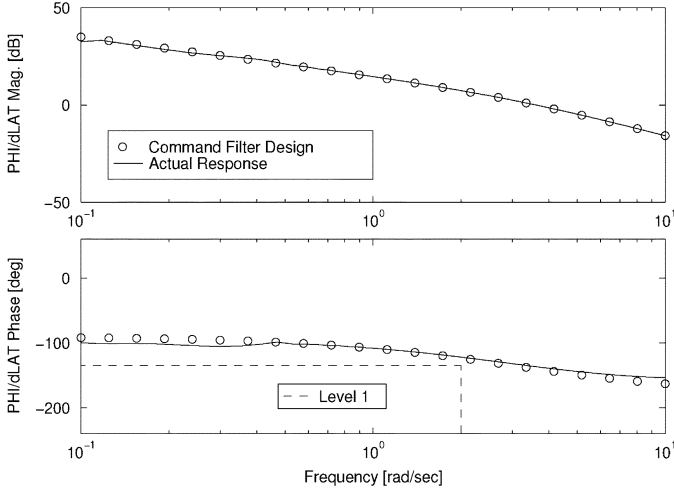


Fig. 14. Roll attitude stick transfer function frequency response at cruise flight. The magnitude of the stick deflection covers 10% of total travel, representative under these conditions, compared with a Bode-plot of the command filter dynamics. The results from the spectrum analysis match the command filter for all frequencies of interest, and the augmentation satisfies the Level 1 bandwidth requirements.

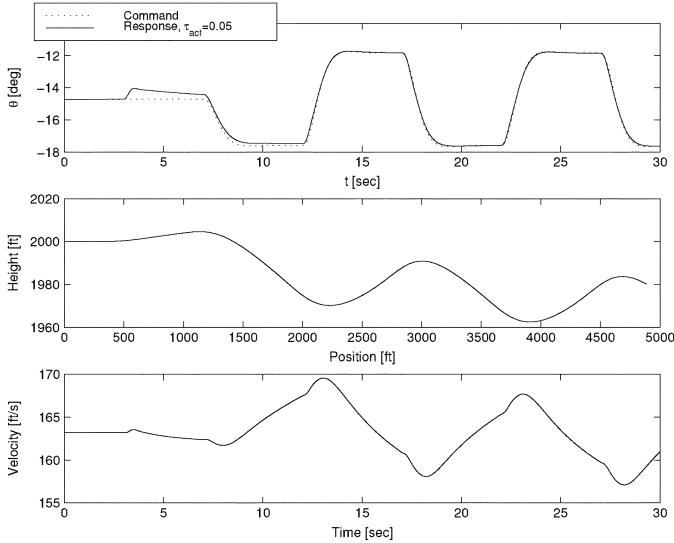


Fig. 15. Aircraft states and tracking performance at 100 Kts helicopter configuration. The aircraft control is “released” at  $t = 2$  s. The model inversion architecture is activated at  $t = 3$  s.

NN. The maneuver provides for a demonstration of operation away from the nominal operating point, visible as the tracking error, and in terms of inversion error in Fig. 16. This figure includes the NN output, which compensates for the inversion error  $\hat{f}_\theta$  (dotted line), as indicated in (25).

## VI. CONCLUSION AND FURTHER WORK

A controller architecture, which combines adaptive feed-forward NNs with FBL, has been outlined and its effectiveness demonstrated on a tilt rotor aircraft. The boundedness of tracking error and control signals is guaranteed. The architecture can accommodate both linear-in-the-parameters NNs, as well as SHL perceptron networks. Theoretical and experimental

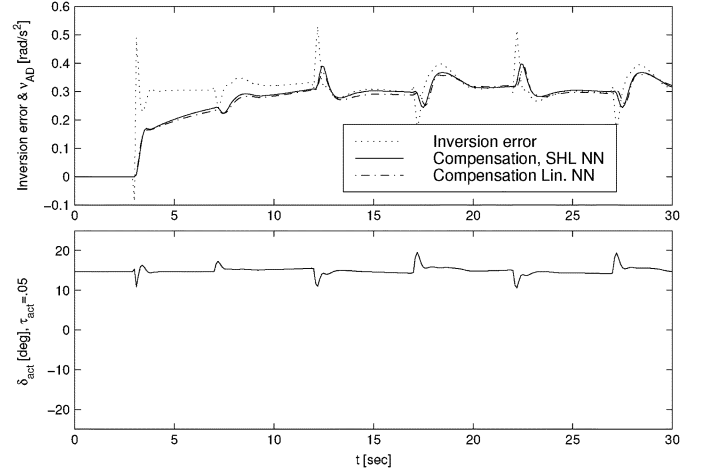


Fig. 16. Inversion error and NN compensation, and actuator activity. The NN weights are initialized with zero weight. The linear NN has  $\gamma = 10$ . The SHL NN robustifying gains were kept relatively small in this demonstration,  $K_{r0} = K_{r1} = K_m = 1.0$  and  $\bar{Z} = 1$ , and  $\gamma_V = 100$  and  $\gamma_W = 100$ . These values provide for a similar response as the linear NN compensation. Though in this demonstration the different NNs performed similarly, other applications have shown the advantages of the more powerful nonlinear NNs [32], [33].

research has shown utility in the areas of cost reduction and improved flight safety.

An important improvement is robustness with respect to actuator dynamics and limits. The adaptive laws may be extended to provide for robustness with respect to unmodeled dynamics [55]. PCH is a powerful extension which may be used to shield the NN adaptation from specific dynamics or actuator limits [47], [56]. PCH allows adaptation-while-saturated, which provides smooth operation when un-saturating. A draw-back of nonlinear adaptive control as presented here is the need for full state feedback. The development of an output feedback formulation is a major extension to the presented work [57], [58].

## APPENDIX I NETWORK INPUT DESIGN

### A. Analysis of the Inversion Error

Similar to (12), concentrating on ACAH in the longitudinal channel, we consider

$$\Delta_{\text{inv}} = \ddot{\theta} - \hat{f}(\theta, \dot{\theta}, \delta_c). \quad (\text{A-1})$$

We use a SHL NN to compensate for  $\Delta_{\text{inv}}$

$$W^{*T} \beta(V^{*T} \bar{\mathbf{x}}) = \Delta_{\text{inv}} - \varepsilon.$$

With the model used for inversion given by

$$\delta_c = \hat{f}^{-1}(\theta, \dot{\theta}, \nu_o)$$

the functional dependency of  $\Delta_{\text{inv}}$  is

$$\begin{aligned} \Delta_{\text{inv}} &\sim \Delta_{\text{inv}}(\theta, \dot{\theta}, \nu_o) \\ &\sim \Delta_{\text{inv}}(\tilde{\theta}, \tilde{\dot{\theta}}, \theta_c, \dot{\theta}_c, \ddot{\theta}_c, \nu_{\text{ad}}, \nu_r). \end{aligned} \quad (\text{A-2})$$

To approximate the inversion error, the NN input should contain all the necessary information. Notice from (A-2) and (44) that

$$\Delta_{\text{inv}} \sim \Delta_{\text{inv}}(\tilde{\theta}, \dot{\tilde{\theta}}, \theta_c, \dot{\theta}_c, \ddot{\theta}_c, \nu_{\text{ad}}, \|Z\|).$$

Therefore, the NN input is chosen as

$$\bar{\mathbf{x}} = [b_V \quad \tilde{\theta} \quad \dot{\tilde{\theta}} \quad \theta_c \quad \dot{\theta}_c \quad \ddot{\theta}_c \quad \nu_{\text{ad}} \quad \|Z\|]^T \quad (\text{A-3})$$

where  $b_V$  is the bias value introduced in (31).

### B. Bound on NN Input

Using

$$\|Z\| = \|Z^* - \tilde{Z}\| \leq \bar{Z} + \|\tilde{Z}\|$$

the NN output may be bounded by

$$\|\nu_{\text{ad}}\| < c'(\bar{Z} + \|\tilde{Z}\|)$$

where  $c' > 0$ . The design as in (A-3), Assumption 2, and Lemma 1 imply

$$\|\bar{\mathbf{x}}\| \leq c'_0 + c'_1|\zeta| + c'_2\|\tilde{Z}\| \quad (\text{A-4})$$

where  $c'_i > 0$ , known.

## APPENDIX II PROOF OF LEMMA 1

Suppose  $\zeta(t) \leq \bar{\zeta}$ , to see how a bounded  $\zeta$  implies bounded elements of  $\mathbf{e}$ , consider (47) as a first-order filter with input  $\zeta$  and output  $\tilde{\theta}$  with feedback gain  $\lambda = P_{12}/P_{22}$ . Then

$$\tilde{\theta}(t) = \frac{1}{P_{22}} \int_0^t e^{-\lambda(t-\tau)} \zeta(\tau) d\tau$$

from which we may conclude

$$\begin{aligned} |\tilde{\theta}(t)| &\leq \frac{\bar{\zeta}}{P_{22}} \int_0^t e^{-\lambda(t-\tau)} d\tau \\ &= \frac{\bar{\zeta}}{P_{22}\lambda} (1 - e^{-\lambda t}) \\ &\leq \frac{\bar{\zeta}}{P_{12}}. \end{aligned} \quad (\text{B-1})$$

Also observe that  $\dot{\tilde{\theta}}(t) = (1/P_{22})\zeta(t) - \lambda\tilde{\theta}(t)$  and, thus, using result (B-1)

$$|\dot{\tilde{\theta}}(t)| \leq \left( \frac{1}{P_{22}} + \frac{\lambda}{P_{12}} \right) \bar{\zeta}(t) \leq \frac{2}{P_{22}} \bar{\zeta}(t). \quad (\text{B-2})$$

Expressions (B-1) and (B-2) allow us to transfer bounds from the signal  $\zeta$ , to the elements of the second-order system (41). Stability of the signal  $\zeta$  implies stability in tracking. Specifically, we can now express the bound on  $\|\mathbf{e}\|$  in terms of  $\bar{\zeta}$ , expression (54).

## APPENDIX III PROOF OF THEOREM 1

The tracking error dynamics are given by

$$\dot{\mathbf{e}} = \mathbf{A}\mathbf{e} + \mathbf{b}(\nu_{\text{ad}} - \Delta_{\text{inv}}). \quad (\text{C-1})$$

Consider the candidate Lyapunov function

$$L(\mathbf{e}, \tilde{W}, \tilde{V}) = \frac{1}{2}\mathbf{e}^T P \mathbf{e} + \frac{1}{2}\tilde{W}^T \Gamma_W^{-1} \tilde{W} + \frac{1}{2}\tilde{V}^T \Gamma_V^{-1} \tilde{V}. \quad (\text{C-2})$$

For  $K_P > 0$  and  $K_D > 0$ ,  $A$  is Hurwitz, and for all  $Q = Q^T > 0$  the solution of

$$A^T P + P A = -Q \quad (\text{C-3})$$

is  $P = P^T > 0$ .

In the sequel we will consider three cases; we start with a linear NN structure where  $V \equiv I$  and let the Lyapunov analysis lead to an idealized update law. Next we introduce the use of an e-modification to the update law which prevents parameter drift in the absence of persistency of excitation (PE), and finally apply a similar approach to the nonlinearly parameterized NN.

*Case 1:* Differentiating (C-2), substituting (33), and using (C-3), gives

$$\begin{aligned} \dot{L} = -\mathbf{e}^T Q \mathbf{e} + \zeta \{ W^T \boldsymbol{\beta}(\mathbf{z}) - W^{*T} \boldsymbol{\beta}^*(\mathbf{z}) - \varepsilon(\mathbf{z}) \} \\ + \tilde{W}^T \Gamma_W^{-1} \dot{\tilde{W}} + \tilde{V}^T \Gamma_V^{-1} \dot{\tilde{V}} \end{aligned} \quad (\text{C-4})$$

where the scalar  $\zeta$  was defined in (47). With  $V \equiv I$  and, thus,  $\dot{\tilde{V}} = \dot{V} \equiv 0$ , (C-4) is reduced to

$$\dot{L} = -\mathbf{e}^T Q \mathbf{e} - \zeta \varepsilon + \tilde{W}^T \left\{ \zeta \boldsymbol{\beta} + \Gamma_W^{-1} \dot{\tilde{W}} \right\}. \quad (\text{C-5})$$

For convenience of analysis choose  $Q = I$ . Observe that

$$\mathbf{e}^T P \mathbf{e} \leq \bar{\lambda}_P \|\mathbf{e}\|^2 \Rightarrow -\mathbf{e}^T \mathbf{e} = -\|\mathbf{e}\|^2 \leq -\frac{\mathbf{e}^T P \mathbf{e}}{\bar{\lambda}_P}$$

where  $\bar{\lambda}_P$  signifies the maximum eigenvalue of positive-definite matrix  $P$  and

$$\begin{aligned} |\zeta| &= |\mathbf{e}^T P \mathbf{b}| \\ &\leq \|\mathbf{e}^T \sqrt{P}\| \|\sqrt{P} \mathbf{b}\| \\ &= \sqrt{\|\mathbf{e}^T \sqrt{P}\| \|\sqrt{P} \mathbf{e}\|} \|\sqrt{P} \mathbf{b}\| \\ &\leq \sqrt{\mathbf{e}^T P \mathbf{e}} \sqrt{\bar{\lambda}_P}. \end{aligned} \quad (\text{C-6})$$

With these observations, we may write

$$\begin{aligned} \dot{L} \leq \frac{-\mathbf{e}^T P \mathbf{e}}{\bar{\lambda}_P} \\ + \bar{\varepsilon} \sqrt{\mathbf{e}^T P \mathbf{e}} \sqrt{\bar{\lambda}_P} + \tilde{W}^T \left\{ \zeta \boldsymbol{\beta} + \Gamma_W^{-1} \dot{\tilde{W}} \right\}. \end{aligned} \quad (\text{C-7})$$

This result suggests an update law

$$\dot{\tilde{W}} = \dot{W} = -\Gamma_W \zeta \boldsymbol{\beta}. \quad (\text{C-8})$$

With this update law,  $\dot{L}$  is strictly negative when

$$\sqrt{\mathbf{e}^T P \mathbf{e}} > \bar{\varepsilon} \bar{\lambda}_P^{3/2}. \quad (\text{C-9})$$

Thus,  $\Omega_{\alpha e} \subset B_e^r$ , as defined in (59), is a positively invariant set of (C-1). Furthermore, define

$$\Omega_{\beta e} = \{\mathbf{e} \in B_e^r : \mathbf{e}^T P \mathbf{e} \leq \bar{\varepsilon}^2 \bar{\lambda}_P^3\}.$$

If  $\Omega_{\beta e} \subset \Omega_{\alpha e}$ , this requires that

$$\bar{\varepsilon}^2 \bar{\lambda}_P^3 < \alpha_e.$$

Then the minimum size of  $B_e^r$  can be quantified by

$$r_e^2 > \frac{\bar{\varepsilon}^2 \bar{\lambda}_P^3}{\lambda_P} \quad (\text{C-10})$$

where  $\mathcal{D}_e$  must be sufficiently large, so that  $B_e^r \subset \mathcal{D}_e$ . This is sufficient to show that  $\mathbf{e}(t)$  remains bounded. Furthermore, if the NN output layer is *persistently exciting* (PE) and the aforementioned assumptions are satisfied, this implies boundedness of  $\tilde{W}$  [59]. If  $\bar{\varepsilon} \equiv 0$ , i.e., no approximation error, then  $\Omega_{\beta e}$  reduces to the origin and  $\lim_{t \rightarrow \infty} \mathbf{e}(t) = 0$ . In this idealized case, the fact that the NN is linear in the parameters allows use of the established adaptive control methods [60] to show boundedness of  $\tilde{W}$ , without requirement for the output layer to be PE [59].

*Case 2:* Consider once more (C-5). We now consider the update law of (C-8) augmented with an *e-modification*, and allowing for a pretrained weight matrix  $W_o$ . PE is very hard to provide for all but the most simple NNs. The e-modification corrects the potential parameter drift that may occur in the absence of PE

$$\dot{\tilde{W}} = \dot{W} = -\Gamma_W \{\zeta \beta + \lambda |\zeta| (W - W_o)\}. \quad (\text{C-11})$$

The choice of  $Q = I$  and substitution of this update law results in

$$\dot{L} = -\mathbf{e}^T \mathbf{e} - \zeta \varepsilon - \lambda |\zeta| \tilde{W}^T (W - W_o).$$

Use the known bound  $\|W^* - W_o\| \leq \bar{W}_o$  and note that

$$\begin{aligned} -\tilde{W}^T (W - W_o) &= -\tilde{W}^T (\tilde{W} + W^* - W_o) \\ &= -\|\tilde{W}\|^2 - \tilde{W}^T (W^* - W_o) \\ &\leq -\|\tilde{W}\|^2 + \|\tilde{W}\| \bar{W}_o. \end{aligned} \quad (\text{C-12})$$

Therefore

$$\begin{aligned} \dot{L} &\leq -\frac{\mathbf{e}^T P \mathbf{e}}{\lambda_P} \\ &\quad -|\zeta| \{\lambda \|\tilde{W}\|^2 - \lambda \|\tilde{W}\| \bar{W}_o\} + |\zeta| \bar{\varepsilon} \end{aligned}$$

which may be rearranged as a quadratic form

$$\begin{aligned} \dot{L} &\leq -\frac{\mathbf{e}^T P \mathbf{e}}{\lambda_P} \\ &\quad -|\zeta| \left\{ \lambda (\|\tilde{W}\| - \bar{W}_o/2)^2 - \bar{\varepsilon} - \lambda \bar{W}_o^2/4 \right\}. \end{aligned} \quad (\text{C-13})$$

This is negative either when

$$\|\tilde{W}\| > \sqrt{\bar{\varepsilon}/\lambda + \bar{W}_o^2/4} + \bar{W}_o/2 \quad (\text{C-14})$$

or when

$$\mathbf{e}^T P \mathbf{e} > \bar{\lambda}_P^3 (\bar{\varepsilon} + \lambda \bar{W}_o^2/4)^2 \quad (\text{C-15})$$

which follows from inequality (C-6) as:

$$\begin{aligned} \mathbf{e}^T P \mathbf{e} / \bar{\lambda}_P &> |\zeta| (\bar{\varepsilon} + \lambda \bar{W}_o^2/4) \\ \Leftrightarrow \mathbf{e}^T P \mathbf{e} / \bar{\lambda}_P &> \sqrt{\mathbf{e}^T P \mathbf{e}} \sqrt{\bar{\lambda}_P} (\bar{\varepsilon} + \lambda \bar{W}_o^2/4) \end{aligned}$$

Then for  $\Omega_\beta \subset \Omega_\alpha$ , the minimum size of  $B^r$  is quantified by (64).

*Case 3:* Consider a Lyapunov function

$$\begin{aligned} L(\mathbf{e}, \tilde{V}, \tilde{W}) &= \frac{1}{2} \mathbf{e}^T P \mathbf{e} + \frac{1}{2\gamma_V} \text{trc}(\tilde{V}^T \tilde{V}) \\ &\quad + \frac{1}{2} \text{trc}(\tilde{W}^T \Gamma_W^{-1} \tilde{W}). \end{aligned}$$

By substituting the update laws (45) and (46) and using previously introduced definition for  $Z$ , the derivative with respect to time of this expression may be expressed as

$$\dot{L} = -\mathbf{e}^T Q \mathbf{e} + \zeta(\nu_r + w) - \lambda |\zeta| \text{trc}(\tilde{Z}^T (Z - Z_o)).$$

Similarly to (C-12)

$$-\tilde{Z}^T (Z - Z_o) \leq -\|\tilde{Z}\|^2 + \|\tilde{Z}\| \bar{Z}_o$$

Therefore

$$\begin{aligned} \dot{L} &\leq -\frac{\mathbf{e}^T P \mathbf{e}}{\lambda_P} + |\zeta| |w| - K_r (\|Z\| + \bar{Z}_o) \zeta^2 \\ &\quad -\lambda |\zeta| \|\tilde{Z}\|^2 + \lambda |\zeta| \|\tilde{Z}\| \bar{Z}_o. \end{aligned}$$

Substitution of the bound on  $w$ , (56), and reordering

$$\begin{aligned} \dot{L} &\leq -\frac{\mathbf{e}^T P \mathbf{e}}{\lambda_P} + c_0 |\zeta| + (c_1 + \lambda \bar{Z}_o) |\zeta| \|\tilde{Z}\| \\ &\quad + (c_2 - \lambda) |\zeta| \|\tilde{Z}\|^2 + \{c_3 \|\tilde{Z}\| - K_r (\|Z\| + \bar{Z}_o)\} |\zeta|^2. \end{aligned}$$

With  $K_r > c_3$  and further reordering

$$\begin{aligned} \dot{L} &\leq -\frac{\mathbf{e}^T P \mathbf{e}}{\lambda_P} \\ &\quad + |\zeta| \{c_0 + (c_1 + \lambda \bar{Z}_o) \|\tilde{Z}\| + (c_2 - \lambda) \|\tilde{Z}\|^2\} \end{aligned}$$

This can be written as a quadratic form

$$\dot{L} \leq -\frac{\mathbf{e}^T P \mathbf{e}}{\lambda_P} + |\zeta| \{(c_2 - \lambda) (\|\tilde{Z}\| - a)^2 - b\}$$

where  $a = (c_1 + \lambda \bar{Z}_o) / (2(c_2 - \lambda))$ , and  $b = c_0 + (c_2 - \lambda) a^2$ , and with  $\lambda > c_2$ . The Lyapunov function derivative is negative when either

$$\mathbf{e}^T P \mathbf{e} > \bar{\lambda}_P^3 b^2 \quad (\text{C-16})$$

or

$$\|\tilde{Z}\| > \sqrt{a^2 + \frac{c_0}{\lambda - c_2}} + a \quad (\text{C-17})$$

which leads to expressions (62) and (63), respectively.  $\square$ 

## REFERENCES

- [1] J. S. Brinker and K. A. Wise, "Flight testing of reconfigurable control law on the x-36 tailless aircraft," *AIAA J. Guid. Control Dyn.*, vol. 24, no. 5, pp. 903–909, Sep.–Oct. 2001.
- [2] A. Isidori, *Nonlinear Control Systems*. Berlin, Germany: Springer-Verlag, 1989.
- [3] G. Meyer and L. Cicolani, "Application of nonlinear systems inverses to automatic flight control design system concepts and flight evaluations," in *Proc. AGARDograph AG-251 on Theory and Applications of Optimal Control in Aerospace Systems*, NATO, 1980, pp. 10-1–10-29.
- [4] P. Menon, G. Chatterji, and V. Cheng, "Two-time-scale autopilot for high performance aircraft," in *Proc. AIAA Guidance, Navigation, and Control Conf.*, 1991. Paper no. AIAA 91-2674.
- [5] N. H. Getz, "Dynamic inversion of nonlinear maps with applications to nonlinear control and robotics," Ph.D. dissertation, Dept. Elect. Eng. and Comp. Sci., Univ. California at Berkeley, 1995.
- [6] D. J. Bugajski, D. F. Enns, and M. R. Elgersma, "A dynamic inversion based control law with application to the high angle of attack research vehicle," in *Proc. AIAA Guidance, Navigation, and Control Conf.*, 1990, pp. 20–22.
- [7] S. A. Snell, D. F. Enns, and W. L. Garrard, "Nonlinear inversion flight control for a supermaneuverable aircraft," *AIAA J. Guid. Control Dyn.*, vol. 15-4, pp. 976–984, 1992.
- [8] J. M. Buffington, A. G. Sparks, and S. S. Banda, "Full conventional envelope longitudinal axis flight control with thrust vectoring," in *Proc. Amer. Control Conf.*, 1993, pp. 415–419.
- [9] J. S. Brinker and K. A. Wise, "Stability and flying qualities robustness of a dynamic inversion aircraft control law," *AIAA J. Guid. Control Dyn.*, vol. 19-6, pp. 1270–1277, 1996.
- [10] R. J. Adams and S. S. Banda, "An integrated approach to flight control design using dynamic inversion and  $\mu$ -synthesis," in *Proc. Amer. Control Conf.*, 1993, pp. 1385–1389.
- [11] J. M. Buffington, R. J. Adams, and S. S. Banda, "Robust nonlinear high angle of attack control design for a supermaneuverable vehicle," in *Proc. AIAA Guidance, Navigation, and Control Conf.*, 1993, pp. 690–700.
- [12] H. Khalil, *Nonlinear Systems*. New York: MacMillan, 1992.
- [13] K. S. Narendra, Y. H. Lin, and L. S. Valavani, "Stable adaptive controller design, part 1 & 2, and stable discrete adaptive control," *IEEE Trans. Autom. Control*, vol. 25, no. 3, pp. 433–461, Jun. 1980.
- [14] S. S. Sastry and A. Isidori, "Adaptive control of linearizable systems," *IEEE Trans. Autom. Control*, vol. 34, no. 11, pp. 1123–1131, Nov. 1989.
- [15] I. Kanellakopoulos, P. V. Kokotovic, and A. S. Morse, "Systematic design of adaptive controllers for feedback linearizable systems," *IEEE Trans. Autom. Control*, vol. 36, no. 11, pp. 1241–1253, Nov. 1991.
- [16] B. B. Peterson and K. S. Narendra, "Bounded error adaptive control," *IEEE Trans. Autom. Control*, vol. AC-27, no. 6, pp. 1162–1168, Dec. 1982.
- [17] S. M. Naik, P. R. Kumar, and B. E. Ydstie, "Robust continuous-time adaptive control by parameter projection," *IEEE Trans. Autom. Control*, vol. 37, no. 2, pp. 182–197, Feb. 1992.
- [18] Y. Zhang and P. A. Ioannou, "Stability and performance of nonlinear robust adaptive control," in *Proc. 34th Conf. Decision Control*, 1995, pp. 3941–3946.
- [19] S. Gopalswamy and J. K. Hedrick, "Robust adaptive nonlinear control of high performance aircraft," in *Proc. Amer. Control Conf.*, 1990, pp. 1279–1283.
- [20] P. V. Kokotovic, "The joy of feedback: Nonlinear and adaptive," *IEEE Control Systems*, vol. 12, no. 3, pp. 7–17, Jun. 1992.
- [21] M. Krstic, J. Sun, and P. V. Kokotovic, "Control of feedback linearizable systems with input unmodeled dynamics," in *Proc. 33rd Conf. Decision Control*, 1994, pp. 1633–1638.
- [22] P. V. Kokotovic and R. A. Freeman, "Robust integral control for a class of uncertain nonlinear systems," in *Proc. 34th Conf. Decision Control*, 1995, pp. 2245–2250.
- [23] K. Funahashi, "On the approximate realization of continuous mappings by neural networks," *Neural Netw.*, vol. 2, pp. 183–192, 1989.
- [24] K. Hornik, M. Stinchcombe, and H. White, "Multilayer feedforward networks are universal approximators," *Neural Netw.*, vol. 2, pp. 359–366, 1989.
- [25] P. J. Werbos, "Neural networks and flight control: Overview of capabilities and emerging applications," in *Proc. AIAA Guidance, Navigation, and Control Conf.*, 1995, pp. 912–919.
- [26] M. Steinberg, "Potential role of neural networks and fuzzy logic in flight control design and development," in *Proc. AIAA Aerospace Design Conf.*, Irvine, CA, 1992. Paper no. AIAA 92-0999.
- [27] —, "An initial assessment of neural network and fuzzy logic technology for flight control systems," in *Proc. Amer. Control Conf.*, 1994, pp. 173–177.
- [28] J. Leitner, A. J. Calise, and J. V. R. Prasad, "Analysis of adaptive neural networks for helicopter flight controls," *AIAA J. Guid. Control Dyn.*, vol. 20, no. 5, pp. 972–979, Sep.–Oct. 1997.
- [29] T. Jiang, J. V. R. Prasad, and A. J. Calise, "Adaptive fuzzy logic flight controller for rotorcraft," in *Proc. AIAA Guidance, Navigation, and Control Conf.*, 1996. Paper no. AIAA 96-3850.
- [30] R. T. Rysdyk and A. J. Calise, "Adaptive model inversion flight control for tiltrotor aircraft," *AIAA J. Guid. Control Dyn.*, 1998.
- [31] R. T. Rysdyk, A. J. Calise, and R. T. N. Chen, "Nonlinear adaptive control of tiltrotor aircraft using neural networks," in *Proc. AIAA/SAE World Aviation Congr.*, Anaheim, CA, Oct. 1997. Paper no. 97-5613.
- [32] B. S. Kim and A. J. Calise, "Nonlinear flight control using neural networks," *AIAA J. Guid. Control Dyn.*, vol. 20-1, pp. 26–33, 1997.
- [33] A. J. Calise, S. Lee, and M. Sharma, "Direct adaptive reconfigurable control of a tailless fighter aircraft," in *Proc. AIAA Guidance, Navigation, and Control Conference*, Boston, MA, Aug. 1998. Paper no. AIAA 98-4108.
- [34] M. B. McFarland and A. J. Calise, "Nonlinear adaptive control of agile anti-air missiles using neural networks," in *Proc. AIAA Missile Sciences Conf.*, Monterey, CA, Dec. 1996. Paper no. AIAA 96-3914.
- [35] M. B. McFarland, R. Rysdyk, and A. J. Calise, "Robust adaptive control using single hidden layer feedforward neural networks," in *Proc. Amer. Control Conf.*, San Diego, CA, Jun. 1999, pp. 4178–4182.
- [36] A. J. Calise, M. Sharma, and J. E. Corban, "An adaptive autopilot design for guided munitions," in *Proc. AIAA Guidance, Navigation, and Control Conf.*, Boston, MA, Aug. 1998. Paper no. AIAA 98-4490.
- [37] E. Gilbert and I. J. Ha, "An approach to nonlinear feedback control with applications in robotics," *IEEE Trans. Syst. Man, Cybern.*, vol. SMC-14, p. 879, 1984.
- [38] M. W. Hirsch and S. Smale, *Differential Equations, Dynamic Systems, and Linear Algebra*. New York: Academic, 1974.
- [39] R. Su, G. Meyer, and L. R. Hunt, *Differential Geometric Control Theory*, R. W. Brockett, R. S. Millman, and H. J. Sussman, Eds. Boston, MA: Birkhauser, 1983, ch. Robustness in Nonlinear Control, p. 316.
- [40] G. Meyer, R. Su, and L. R. Hunt, "Applications of nonlinear transformations to automatic flight control," *Automatica*, vol. 20, pp. 103–107, 1984.
- [41] J. Hauser, S. Sastry, and G. Meyer, "Nonlinear control design for slightly nonminimum phase systems: Application to v/stol aircraft," *Automatica*, vol. 28, no. 4, pp. 665–679, 1992.
- [42] S. Bharadwaj, A. V. Rao, and K. D. Mease, "Entry trajectory tracking law via feedback linearization," *J. Guid. Navigat. Control*, vol. 21, no. 5, pp. 726–732, 1998.
- [43] *Handling Qualities Requirements for Military Rotorcraft, ADS-33D*, Jul. 1994. Aeronautical Design Standard.
- [44] W. A. Decker, "Piloted simulator investigations of a civil tiltrotor aircraft on steep instrument approaches," in *Proc. AHS 48th Annu. Forum*, Washington, DC, Jun. 1992.
- [45] B. Etkin, *Dynamics of Atmospheric Flight*. New York: Wiley, 1972.
- [46] B. L. Stevens and F. L. Lewis, *Aircraft Control and Simulation*. New York: Wiley, 1992.
- [47] E. Johnson, A. J. Calise, H. El-Shirbiny, and R. Rysdyk, "Feedback linearization with neural network augmentation applied to x33 attitude control," in *Proc. AIAA Guidance, Navigation, Control Conf.*, vol. Denver, 2000.
- [48] R. M. Sanner and J. E. Slotine, "Gaussian networks for direct adaptive control," *IEEE Trans. Neural Netw.*, vol. 3, no. 6, pp. 837–863, Nov. 1992.
- [49] A. Yesildirek and F. L. Lewis, "Feedback linearization using neural networks," *Automatica*, vol. 31, no. 11, pp. 1659–1664, 1995.
- [50] A. J. Calise, S. Lee, and M. Sharma, "Development of a reconfigurable flight control law for the tailless aircraft," *AIAA J. Guid. Control Dyn.*, vol. 24, no. 5, pp. 896–902, Oct. 2000.
- [51] "A Mathematical Model for Real Time Flight Simulation of a Generic Tilt-Rotor Aircraft," NASA CR-166 536 Rev. A, Sep. 1988.

- [52] M. B. McFarland and A. J. Calise, "Multilayer neural networks and adaptive nonlinear control of agile anti-air missiles," in *Proc. AIAA Guidance, Navigation, and Control Conf.*, vol. AIAA 97-3540, 1997.
- [53] A. J. Calise and R. T. Rysdyk, "Research in Nonlinear Flight Control for Jiltrotor Aircraft Operating in the Terminal Area," vol. NASA NCC 2-922, Nov. 1996.
- [54] R. T. Rysdyk and A. J. Calise, "Adaptive nonlinear flight control for consistent handling qualities," in *Proc. AHS 54th Annu. Forum*, Washington, DC, Jun. 1998.
- [55] R. T. Rysdyk, "Adaptive nonlinear flight control," Ph.D. dissertation, School Aerosp. Eng., Georgia Inst. Technol., Atlanta, GA, 1998.
- [56] E. N. Johnson and A. J. Calise, Neural Network Adaptive Control of Systems with Input Saturation.
- [57] N. Hovakimyan and A. J. Calise, "Adaptive output feedback control of uncertain multi-input multi-output systems using single hidden layer neural networks," *Proc. Amer. Control Conf.*, pp. 1555–1560, 2002.
- [58] A. J. Calise, N. Hovakimyan, and M. Idan, "Adaptive output feedback control of nonlinear systems using neural networks," *Automatica*, vol. 37, no. 8, pp. 1201–1211, Aug. 2001.
- [59] F. L. Lewis, "Nonlinear network structures for feedback control," *Asian J. Control*, vol. 1, no. 4, pp. 205–228, 1999.
- [60] M. Krstic, I. Kanellakopoulos, and P. V. Kokotovic, *Nonlinear and Adaptive Control Design*. New York: Wiley, 1995.



**Rolf Rysdyk** studied at the Delft University of Technology, Delft, the Netherlands, working with the Delft research flight simulator for proprioception and motion cues experiments.

He is currently an Assistant Professor in the Department of Aeronautics and Astronautics, University of Washington, Seattle. After graduation, he moved to the United States and performed duties as a commercial pilot. Subsequently, he enrolled at the Georgia Institute of Technology, Atlanta, where Dr. A. J. Calise asked him to demonstrate nonlinear adaptive control for consistent handling qualities on a tiltrotor aircraft, which formed the focus of his Ph.D. dissertation research, leading to theoretical developments that were motivated by real world control design challenges from Industry and Government. This work included application to propulsion only control of transport aircraft, with *a priori* methods to deal with actuator saturation. More recently, he focused on the control of multiple UAVs in a highly dynamic environment; specifically, combined task and path planning and mission tactical maneuvers for payload optimization.



**Anthony J. Calise** (S'63–M'74–SM'04) was a Professor of Mechanical Engineering at Drexel University, Philadelphia, PA, for eight years prior to joining the faculty at the Georgia Institute of Technology, Atlanta. He also worked for ten years in industry for the Raytheon Missile Systems Division and Dynamics Research Corporation, where he was involved with analysis and design of inertial navigation systems, optimal missile guidance, and aircraft flight path optimization. Since leaving industry, he has worked continuously as a consultant

for 19 years. He is the author of over 150 technical reports and papers. The subject areas that he has published in include optimal control theory, aircraft flight control, optimal guidance of aerospace vehicles, adaptive control using neural networks, robust linear control, and control of flexible structures. In the area of adaptive control, he has developed a novel combination for employing neural-network-based control in combination with feedback linearization. Applications include flight control of fighter aircraft, helicopters, and missile autopilot design. He is a former Associate Editor for the *Journal of Guidance, Control, and Dynamics*.

Dr. Calise was the recipient of the USAF Systems Command Technical Achievement Award, and the AIAA Mechanics and Control of Flight Award. He is a Fellow of the AIAA and an Associate Editor for the *IEEE Control Systems Magazine*.